8

Sliding-Mode Control of Switched-Mode Power Supplies

Giorgio Spiazzi
University of Padova

Paolo Mattavelli
University of Padova

Switch-mode power supplies represent a particular class of variable structure systems (VSS), and they can take advantage of nonlinear control techniques developed for this class of system. Sliding-mode control, which is derived from variable structure system theory [1, 2], extends the properties of hysteresis control to multivariable environments, resulting in stability even for large supply and load variations, good dynamic response, and simple implementation.

Some basic principles of sliding-mode control are first reviewed. Then the application of the sliding-mode control technique to DC-DC converters is described. The application to buck converter is discussed in detail, and some guidelines for the extension of this control technique to boost, buck–boost, Cúk, and SEPIC converters are given. Finally, to overcome some inherent drawbacks of sliding-mode control, improvements like current limitation, constant switching frequency, and output voltage steady-state error cancellation are described.

8.1 Introduction

Switch-mode power supplies (SMPS) are nonlinear and time-varying systems, and thus the design of a high-performance control is usually a challenging issue. In fact, control should ensure system stability in any operating condition and good static and dynamic performances in terms of rejection of input voltage disturbances and load changes. These characteristics, of course, should be maintained in spite of large input voltage, output current, and even parameter variations (robustness).

A classical control approach relies on the *state space averaging* method, which derives an equivalent model by circuit-averaging all the system variables in a switching period [3–5]. On the assumptions that the switching frequency is much greater than the natural frequency of system variables, low-frequency dynamics is preserved while high-frequency behavior is lost. From the average model, a suitable small-signal model is then derived by perturbation and linearization around a precise operating point. Finally, the small-signal model is used to derive all the necessary converter transfer functions to design a linear control system by using classical control techniques. The design procedure is well known, but it is generally not easy to account for the wide variation of system parameters, because of the strong dependence of small-signal model parameters on the converter operating point. Multiloop control techniques, such as current-mode control, have greatly improved power converter dynamic behavior, but the control design remains difficult especially for high-order topologies, such as those based on Cúk and SEPIC schemes.

The sliding-mode approach for variable structure systems (VSS) [1, 2] offers an alternative way to implement a control action that exploits the inherent variable structure nature of SMPS. In particular, the converter switches are driven as a function of the instantaneous values of the state variables to force the system trajectory to stay on a suitable selected surface on the phase space. This control technique offers several advantages in SMPS applications [6–19]: stability even for large supply and load variations, robustness, good dynamic response, and simple implementation. Its capabilities emerge especially in application to high-order converters, yielding improved performances as compared with classical control techniques.

In this chapter, some basic principles of sliding-mode control are reviewed in a tutorial manner and its applications to DC-DC converters are investigated. The application to buck converters is first discussed in details, and then guidelines for the extension of this control technique to boost, buck–boost, Cúk, and SEPIC converters are given. Finally, improvements like current limitation, constant switching frequency, and output voltage steady-state error cancellation are discussed.

8.2 Introduction to Sliding-Mode Control

Sliding-mode control is a control technique based on VSS, defined as systems where the circuit topology is intentionally changed, following certain rules, to improve the system behavior in terms of speed of response, stability, and robustness. A VSS is based on a defined number of independent subtopologies, which are defined by the status of nonlinear elements (switches); the global dynamics of the system is, however, substantially different from that of each single subtopology. The theory of VSS [1, 2] provides a systematic procedure for the analysis of these systems and for the selection and design of the control rules. To introduce sliding-mode control, a simple example of a second-order system is analyzed. Two different substructures are introduced and a combined action, which defines a sliding mode, is presented. The first substructure, which is referred as substructure I, is given by the following equations:

$$\begin{cases} \dot{x}_1 = x_2 \\ \dot{x}_2 = -K \cdot x_1 \end{cases} \tag{8.1}$$

where the eigenvalues are complex with zero real part; thus, for this substructure the phase trajectories are circles, as shown in Fig. 8.1 and the system is marginally stable. The second substructure, which is

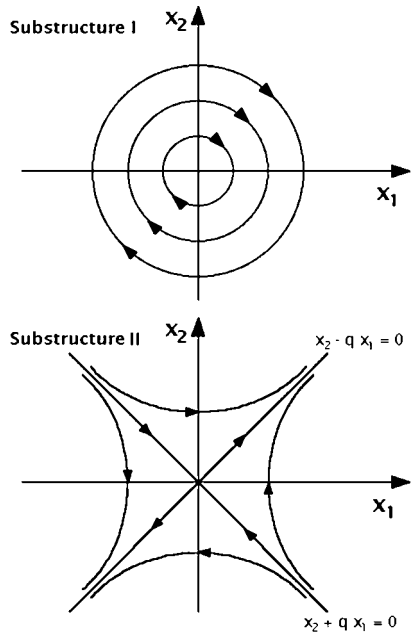

FIGURE 8.1 Phase-plane description corresponding to substructures I and II.

referred as substructure II, is given by

$$\begin{cases} \dot{x}_1 = x_2 \\ \dot{x}_2 = +K \cdot x_1 \end{cases} \tag{8.2}$$

In this case the eigenvalues are real and with opposite sign; the corresponding phase trajectories are shown in Fig. 8.1 and the system is unstable. Only one phase trajectory, namely, $x_2 = -qx_1 (q = \sqrt{K})$, converges toward the origin, whereas all other trajectories are divergent.

Divide the phase-plane in two regions, as shown in Fig. 8.2; accordingly, at each region is associated one of the two substructures as follows:

Region I: $x_1 \cdot (x_2 + cx_1) < 0 \Rightarrow$ Substructure I
Region II: $x_1 \cdot (x_2 + cx_1) > 0 \Rightarrow$ Substructure II

where c is lower than q. The switching boundaries are the x_2 axis and the line $x_2 + cx_1 = 0$. The system structure changes whenever the system representative point (RP) enters a region defined by the switching boundaries. The important property of the phase trajectories of both substructures is that, in the vicinity of the switching line $x_2 + cx_1 = 0$, they converge to the switching line. The immediate consequence of this property is that, once the RP hits the switching line, the control law ensures that the RP does not move away from the switching line. Figure 8.2a shows a typical overall trajectory starting from an arbitrary initial condition $P_0 (x_{10}, x_{20})$: after the intervals corresponding to trajectories $P_0 - P_1$ (substructure I) and $P_1 - P_2$ (substructure II), the final state evolution lies on the switching line (in the hypothesis of ideal infinite frequency commutations between the two substructures).

This motion of the system RP along a trajectory, on which the structure of the system changes and which is not part of any of the substructure trajectories, is called the *sliding mode*, and the switching line $x_2 + cx_1 = 0$ is called the *sliding line*. When sliding mode exists, the resultant system performance is completely different from that dictated by any of the substructures of the VSS and can be, under particular conditions, made independent of the properties of the substructures employed and dependent only on

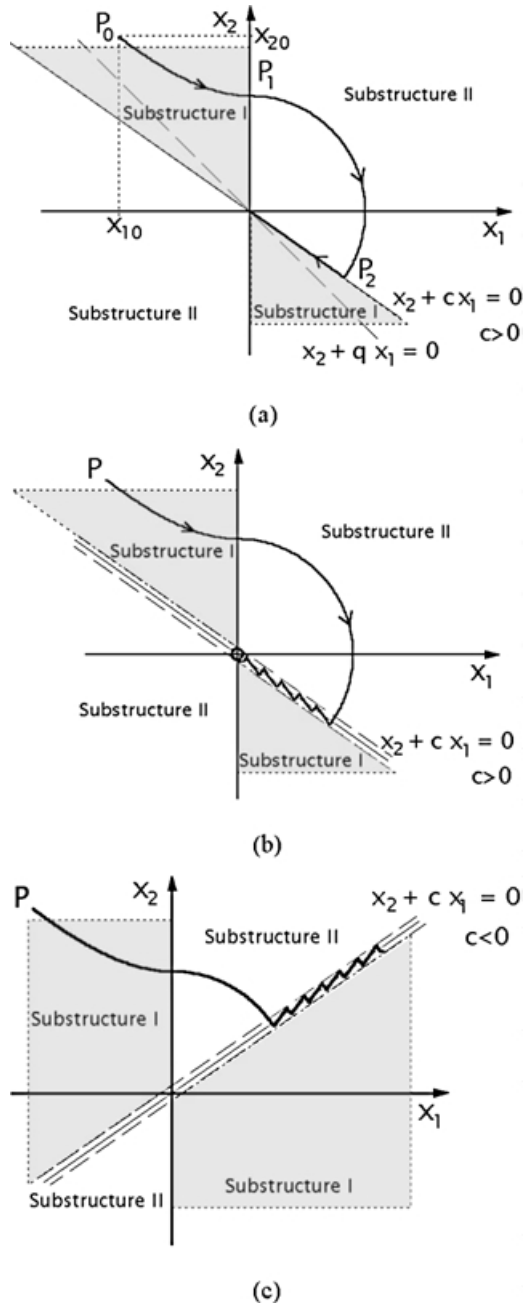

FIGURE 8.2 Sliding regime in VSS. (a) Ideal switching line; (b) switching line with hysteresis; (c) unstable sliding mode.

the control law (in this example the boundary $x_2 + cx_1 = 0$). In this case, for example, the dynamic is of the first order with a time constant equal to $1/c$.

The independence of the closed-loop dynamics on the parameters of each substructure is not usually true for more complex systems, but even in these cases it has been proved that the sliding-mode control maintains good robustness compared with other control techniques. For higher-order systems, the control

rule can be written in the following way:

$$\sigma = f(x_1, \ldots, x_N) = \sum_{i=1}^{N} c_i x_i = 0 \tag{8.3}$$

where N is the system order and x_i are the state variables. Note that the choice of using a linear combination of state variable in Eq. (8.3) is only one possible solution, which results in a particularly simple implementation in SMPS applications.

When the switching boundary is not ideal, i.e., the commutation frequency between the two substructures is finite, then the overall system trajectory is as shown in Fig. 8.2b. Of course, the width of the hysteresis around the switching line determines the switching frequency between the two substructures.

Following this simple example and looking at the Figs. 8.1 and 8.2, it is easy to understand that the conditions for realizing a sliding-mode control are:

- *Existence condition*: The trajectories of the two substructures are directed toward the sliding line when they are close to it.
- *Hitting condition*: Whatever the initial conditions, the system trajectories must reach the sliding line.
- *Stability condition*: The evolution of the system under sliding mode should be directed to a stable point. In Fig. 8.2b the system in sliding mode goes to the origin of the system, that is, a stable point. But if the sliding line were the following:

Region I: $x_1 \cdot (x_2 + cx_1) < 0 \Rightarrow$ Substructure I
Region II: $x_1 \cdot (x_2 + cx_1) > 0 \Rightarrow$ Substructure II

where $c < 0$, then the system trajectories would have been as shown in Fig. 8.2c. In this case, the resulting state trajectory still follows the sliding line, but it goes to infinity and the system is therefore unstable.

The approach to more complex systems cannot be expressed only with graphical considerations, and a mathematical approach should be introduced, as reported below.

8.3 Basics of Sliding-Mode Theory

Consider the following general system with scalar control [1, 2]:

$$\dot{\mathbf{x}} = \mathbf{f}(\mathbf{x}, t, u) \tag{8.4}$$

where $\mathbf{x}$ is a column vector and $\mathbf{f}$ is a function vector, both of dimension N, and u is an element that can influence the system motion (control input). Consider that the function vector $\mathbf{f}$ is discontinuous on a surface $\sigma(\mathbf{x}, t) = 0$. Thus, one can write:

$$\mathbf{f}(\mathbf{x}, t, u) = \begin{cases} \mathbf{f}^+(\mathbf{x}, t, u^+) & \text{for} \quad \sigma \to 0^+ \\ \mathbf{f}^-(\mathbf{x}, t, u^-) & \text{for} \quad \sigma \to 0^- \end{cases} \tag{8.5}$$

where the scalar discontinuous input u is given by

$$u = \begin{cases} u^+ & \text{for} \quad \sigma(\mathbf{x}) > 0 \\ u^- & \text{for} \quad \sigma(\mathbf{x}) < 0 \end{cases} \tag{8.6}$$

The system is in sliding mode if its representative point moves on the sliding surface $\sigma(\mathbf{x}, t) = 0$.

Existence Condition

For a sliding mode to exist, the phase trajectories of the two substructures corresponding to the two different values of the vector function **f** must be directed toward the sliding surface $\sigma(\mathbf{x}, t) = 0$ in a small region close to the surface itself. In other words, approaching the sliding surface from points where $\sigma < 0$, the corresponding state velocity vector $\mathbf{f}^-$ must be directed toward the sliding surface, and the same must happen when points above the surface ($\sigma > 0$) are considered, for which the corresponding state velocity vector is $\mathbf{f}^+$. Indicating with subscript **N** the components of state velocity vectors $\mathbf{f}^+$ and $\mathbf{f}^-$ orthogonal to the sliding surface one can write:

$$\begin{matrix} \lim_{\sigma \to o^+} \mathbf{f}_\mathbf{N}^+ < 0 \\ \lim_{\sigma \to o^-} \mathbf{f}_\mathbf{N}^- > 0 \end{matrix} \Rightarrow \begin{matrix} \lim_{\sigma \to o^+} \nabla\sigma \cdot \mathbf{f}^+ < 0 \\ \lim_{\sigma \to o^-} \nabla\sigma \cdot \mathbf{f}^- > 0 \end{matrix} \tag{8.7}$$

where $\nabla\sigma$ is the gradient of surface σ. Since

$$\frac{d\sigma}{dt} = \sum_{i=1}^{N} \frac{\partial\sigma}{\partial x_i} \frac{dx_i}{dt} = \nabla\sigma \cdot \mathbf{f} \tag{8.8}$$

the existence condition of the sliding mode becomes

$$\begin{matrix} \lim_{\sigma \to o^+} \frac{d\sigma}{dt} < 0 \\ \lim_{\sigma \to o^-} \frac{d\sigma}{dt} > 0 \end{matrix} \Rightarrow \lim_{\sigma \to o} \sigma \frac{d\sigma}{dt} < 0 \tag{8.9}$$

When the inequality given by Eq. (8.9) holds in the entire state space and not only in an infinitesimal region around the sliding surface, then this condition is also a sufficient condition that the system will reach the sliding surface.

Hitting Conditions

Let $[\mathbf{x}^+]$ and $[\mathbf{x}^-]$ be the steady-state RPs corresponding to the inputs u^+ and u^- Eq. (8.6), respectively. Then a simple sufficient condition, that will be used later in the application of the sliding mode control to switch-mode power supplies, for reaching the sliding surface is given by:

$$[\mathbf{x}^+] \in \sigma(\mathbf{x}) < 0, \qquad [\mathbf{x}^-] \in \sigma(\mathbf{x}) > 0 \tag{8.10}$$

In other words, if the steady-state point for one substructure belongs to the region of the phase space reserved to the other substructure, then sooner or later the system RP will hit the sliding surface.

System Description in Sliding Mode: Equivalent Control

The next focus of interest in the analysis of VSS is the behavior of the system operating in sliding regime. Consider here a particular class of systems that are linear with the control input, i.e.,

$$\dot{\mathbf{x}} = \mathbf{f}(\mathbf{x}, t) + \mathbf{B}(\mathbf{x}, t)u \tag{8.11}$$

where $\mathbf{x} \in \Re^N$, **f** and $\mathbf{B} \in \Im^N$, $u \in \Re^1$.

The scalar control input u is discontinuous on the sliding surface $\sigma(\mathbf{x}, t) = 0$, as shown in Eq. (8.6), whereas $\mathbf{f}$ and $\mathbf{B}$ are continuous function vectors. Under sliding mode control, the system trajectories stay on the sliding surface, hence:

$$\sigma(\mathbf{x}, t) = 0 \quad \Rightarrow \quad \sigma(\mathbf{x}, t) = 0 \tag{8.12}$$

$$\dot{\sigma}(\mathbf{x}, t) = \frac{d\sigma}{dt} = \sum_{i=1}^{N} \frac{\partial \sigma}{\partial x_i} \frac{dx_i}{dt} = \nabla \sigma \cdot \dot{\mathbf{x}} = \mathbf{G}\dot{\mathbf{x}} \tag{8.13}$$

where $\mathbf{G}$ is a 1 by N matrix whose elements are the derivatives of the sliding surface with respect to the state variables. By using Eqs. (8.11) and (8.13),

$$\mathbf{G}\dot{\mathbf{x}} = \mathbf{G}\mathbf{f}(\mathbf{x}, t) + \mathbf{G}\mathbf{B}(\mathbf{x}, t)u_{\text{eq}} = 0 \tag{8.14}$$

where the control input u was substituted by an equivalent control u_{eq} that represents an equivalent continuous control input that maintains the system evolution on the sliding surface. On the assumption that $[\mathbf{GB}]^{-1}$ exists, from Eq. (8.14) one can derive the expression for the equivalent control:

$$u_{\text{eq}} = -(\mathbf{GB})^{-1}\mathbf{G}\mathbf{f}(\mathbf{x}, t) \tag{8.15}$$

Finally, by substituting this expression into Eq. (8.11),

$$\dot{\mathbf{x}} = [\mathbf{I} - \mathbf{B}(\mathbf{GB})^{-1}\mathbf{G}]\mathbf{f}(\mathbf{x}, t) \tag{8.16}$$

Equation (8.16) describes the system motion under sliding-mode control. It is important to note that the matrix $\mathbf{I} - \mathbf{B}(\mathbf{GB})^{-1}\mathbf{G}$ is less than full rank. This is because, under sliding regime, the system motion is constrained to be on the sliding surface. As a consequence, the equivalent system described by Eq. (8.16) is of order $N - 1$. This equivalent control description of a VSS in sliding regime is valid, of course, also for multiple control inputs. For details, see Refs. 1 and 2.

Stability

Analyzing the system behavior in the phase-plane for the second-order system, it was found that the system stability is guaranteed if its trajectory, in sliding regime, is directed toward a stable operating point. For higher-order systems, a direct view of the phase space is not feasible and one must prove system stability through mathematical tools. First consider a simple linear system with scalar control in the following canonical form:

$$\begin{cases} \dot{x}_i = x_{i+1} & i = 1, 2, \ldots, N-1 \\ \dot{x}_N = \displaystyle\sum_{j=1}^{N} a_{Nj}x_j + bu \end{cases} \tag{8.17}$$

and

$$\sigma(\mathbf{x}, t) = \sum_{i=1}^{N} c_i x_i = \sum_{i=1}^{N} c_i \frac{d^{i-1}x_1}{dt^{i-1}} = 0 \tag{8.18}$$

The latter equation completely defines the system dynamic in sliding regime. Moreover, in this case the system dynamic in sliding mode depends only on the sliding surface coefficients c_i, leading to a system behavior that is completely different from those given by the substructures defined by the two control

input values u^+ and u^-. This is a highly desirable situation because the system dynamic can be directly determined by a proper c_i selection. Unfortunately, in the application to DC-DC converters this is possible only for the buck topology, whereas for other converters, state derivatives are not only difficult to measure, but also discontinuous. Therefore, we are obliged to select system states that are measurable, physical, and continuous variables. In this general case, the system stability in sliding mode can be analyzed by using the equivalent control method Eq. (8.16).

8.4 Application of Sliding-Mode Control to DC-DC Converters—Basic Principle

The general sliding-mode control scheme of DC-DC converters is shown in Fig. 8.3. U_g and u_o are input and output voltages, respectively, while i_{Li} and u_{Cj} ($i = 1 \div r$, $j = r + 1 \div N - 1$) are the internal state variables of the converter (inductor currents and capacitor voltages). Switch S accounts for the system nonlinearity and indicates that the converter may assume only two linear subtopologies, each associated to one switch status. All DC-DC converters having this property (including all single-switch topologies, plus push-pull, half and two-level full-bridge converters) are represented by the equivalent scheme of Fig. 8.3. The above condition also implies that the sliding-mode control presented here is valid only for *continuous conduction mode* (CCM) of operation.

In the scheme of Fig. 8.3, according to the general sliding-mode control theory, all state variables are sensed, and the corresponding errors (defined by difference to the steady-state values) are multiplied by proper gains c_i and added together to form the sliding function σ. Then, hysteretic block HC maintains this function near zero, so that

$$\sigma = \sum_{i=1}^{N} c_i \varepsilon_i = 0 \tag{8.19}$$

Observe that Eq. (8.19) represents a hyperplane in the state error space, passing through the origin. Each of the two regions separated by this plane is associated, by block HC, to one converter sub structure. If one assumes (*existence condition* of the sliding mode) that the state trajectories near the surface, in both regions,

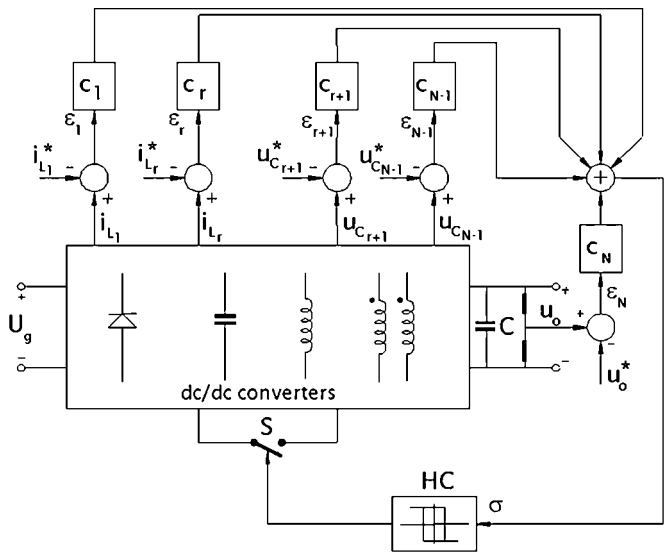

FIGURE 8.3 Principle scheme of a SM controller applied to DC-DC converters.

are directed toward the sliding plane, the system state can be enforced to remain near (lie on) the sliding plane by proper operation of the converter switch(es).

Sliding-mode controller design requires only a proper selection of the sliding surface Eq. (8.19), i.e., of coefficients c_i, to ensure existence, hitting, and stability conditions. From a practical point of view, selection of the sliding surface is not difficult if second-order converters are considered. In this case, in fact, the above conditions can be verified by simple graphical techniques. Instead, for higher-order converters, like Cúk and SEPIC, the more general approach outlined in Section 8.5 must be used.

One of the major problem of the general scheme of Fig. 8.3 is that inductor current and capacitor voltage references are difficult to evaluate, because they generally depend on load power demand, supply voltage, and load voltage. This is true for all basic topologies, except the buck converter, whose dynamic equations can be expressed in canonical form Eq. (8.17). Thus, for all converters, except the buck topology, some provisions are needed for the estimation of such references, strongly affecting the closed-loop dynamics, as discussed in the following sections.

8.5 Sliding-Mode Control of Buck DC-DC Converters

It was already mentioned that one of the most important features of the sliding-mode regimes in VSS is the ability to achieve responses that are independent of system parameters, the only constraint being the canonical form description of the system. From this point of view, the buck DC-DC converter is particularly suitable for the application of the sliding-mode control, because its controllable states (output voltage and its derivative) are all continuous and accessible for measurement.

Phase-Plane Description

The basic buck DC-DC converter topology is shown in Fig. 8.4.

In this case it is more convenient to use a system description, which involves the output error and its derivative, i.e.,

$$\begin{cases} x_1 = u_o - U_o^* \\ x_2 = \dfrac{dx_1}{dt} = \dfrac{du_o}{dt} = \dfrac{i_C}{C} \end{cases} \tag{8.20}$$

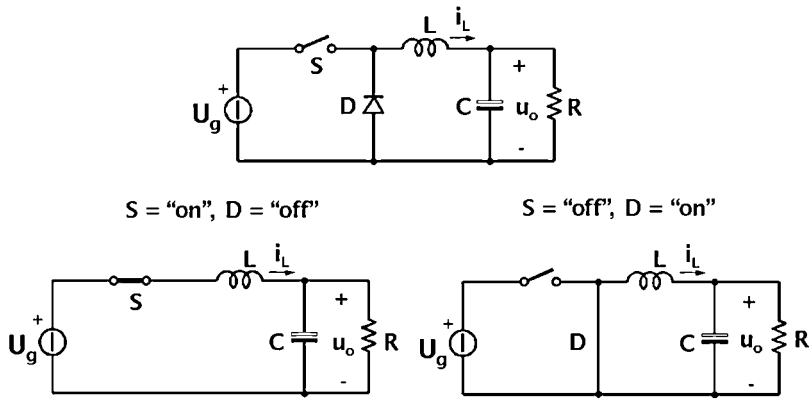

FIGURE 8.4 Buck DC-DC converter topology and related substructures corresponding to two different switch positions.

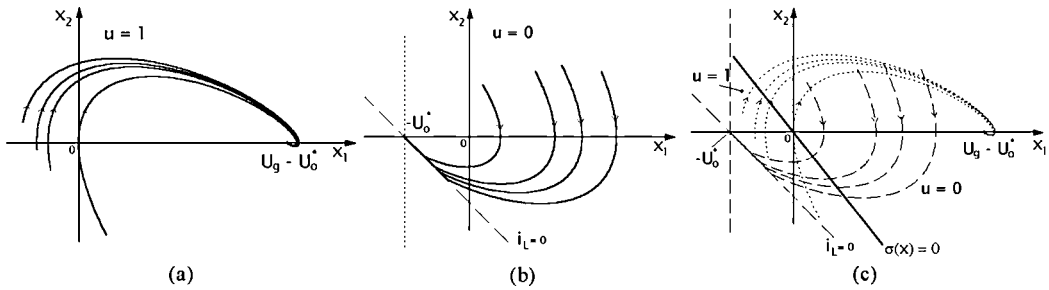

FIGURE 8.5 (a) Phase trajectories of the substructure corresponding to $u = 1$; (b) Phase trajectories of the substructure corresponding to $u = 0$; (c) Subsystem trajectories and sliding line in the phase-plane of the buck converter.

The system equations, in terms of state variables x_1 and x_2 and considering a continuous conduction mode (CCM) operation can be written as

$$\begin{cases} \dot{x}_1 = x_2 \\ \dot{x}_2 = -\dfrac{x_1}{\mathrm{LC}} - \dfrac{x_2}{\mathrm{RC}} + \dfrac{U_g}{\mathrm{LC}}u - \dfrac{U_o^*}{\mathrm{LC}} \end{cases} \tag{8.21}$$

where u is the discontinuous input, which can assume the values 0 (switch OFF) or 1 (switch ON). In state-space form:

$$\begin{aligned} \dot{\mathbf{x}} &= \mathbf{A}\mathbf{x} + \mathbf{B}u + \mathbf{D} \\ \mathbf{A} &= \begin{bmatrix} 0 & 1 \\ -\dfrac{1}{\mathrm{LC}} & -\dfrac{1}{\mathrm{RC}} \end{bmatrix}, \qquad \mathbf{B} = \begin{bmatrix} 0 \\ \dfrac{U_g}{\mathrm{LC}} \end{bmatrix}, \qquad \mathbf{D} = \begin{bmatrix} 0 \\ -\dfrac{U_o^*}{\mathrm{LC}} \end{bmatrix} \end{aligned} \tag{8.22}$$

Practically, the damping factor of this second-order system is less than 1, resulting in complex conjugate eigenvalues with negative real part. The phase trajectories corresponding to the substructure $u = 1$ are shown in Fig. 8.5a for different values of the initial conditions. The equilibrium point for this substructure is $x_{1\mathrm{eq}} = U_g - U_o^*$ and $x_{2\mathrm{eq}} = 0$. Instead, with $u = 0$ the corresponding phase trajectories are reported in Fig. 8.5b and the equilibrium point for this second substructure is $x_{1\mathrm{eq}} = -U_o^*$ and $x_{2\mathrm{eq}} = 0$.

Note that the real structure of Fig. 8.5b has a physical limitation due to the rectifying characteristic of the freewheeling diode. In fact, when the switch S is OFF, the inductor current can assume only non-negative values. In particular, when i_L goes to zero it remains zero and the output capacitor discharge goes exponentially to zero. This situation corresponds to the discontinuous-conduction mode (DCM) and it poses a constraint on the state variables. In other words, part of the phase-plane does not correspond to possible physical states of the system and so need not be analyzed. The boundary of this region can be derived from the constraint $i_L = 0$ and is given by the equation:

$$x_2 = -\frac{1}{\mathrm{RC}}x_1 - \frac{U_o^*}{\mathrm{RC}} \tag{8.23}$$

which corresponds to the straight line with a negative slope equal to $-1/\mathrm{RC}$ and passing through the point $(-U_o^*, 0)$ shown in dashed line in Fig. 8.5b. In the same figure, the line $x_1 = -U_o^*$ is also reported, which defines another not physically accessible region of the phase-plane, i.e., the region in which $u_o < 0$.

Selection of the Sliding Line

It is convenient to select the sliding surface as a linear combination of the state variables because the results are very simple to implement in the real control system and because it allows the use of the equivalent control method to describe the system dynamic in sliding mode. Thus, we can write:

$$\sigma(\mathbf{x}) = c_1 x_1 + x_2 = \mathbf{C}^T \mathbf{x} = 0 \tag{8.24}$$

where $\mathbf{C}^T = [c_1, 1]$ is the vector of sliding surface coefficients which corresponds to **G** in Eq. (8.13), and coefficient c_2 was set to 1 without loss of generality.

As shown in Fig. 8.5c, this equation describes a line in the phase-plane passing through the origin, which represents the stable operating point for this converter (zero output voltage error and its derivative). By using Eq. (8.21), Eq. (8.24) becomes

$$\sigma(\mathbf{x}) = c_1 x_1 + \dot{x}_1 = 0 \tag{8.25}$$

which completely describes the system dynamic in sliding mode. Thus, if existence and reaching conditions of the sliding mode are satisfied, a stable system is obtained by choosing a positive value for c_1. Figure 8.5c reveals the great potentialities of the phase-plane representation for second-order systems. In fact, a direct inspection of Fig. 8.5c shows that if we choose the following control law:

$$u = \begin{cases} 0 & \text{for} \quad \sigma(\mathbf{x}) > 0 \\ 1 & \text{for} \quad \sigma(\mathbf{x}) < 0 \end{cases} \tag{8.26}$$

then both existence and reaching conditions are satisfied, at least in a small region around the system equilibrium point. In fact, we can easily see that, using this control law, for both sides of the sliding line the phase trajectories of the corresponding substructures are directed toward the sliding line (at least in a small region around the origin). Moreover, the equilibrium point for the substructure corresponding to $u = 0$ belongs to the region of the phase-plane relative to the other substructure, and vice versa, thus ensuring the reachability of the sliding line from any allowed initial state condition. From Eq. (8.5) it is easy to see that the output voltage dynamics in sliding mode is simply given by a first-order system with time constant equal to $1/c_1$. Typical waveforms with $c_1 = 0.8/RC$ are reported in Fig. 8.6.

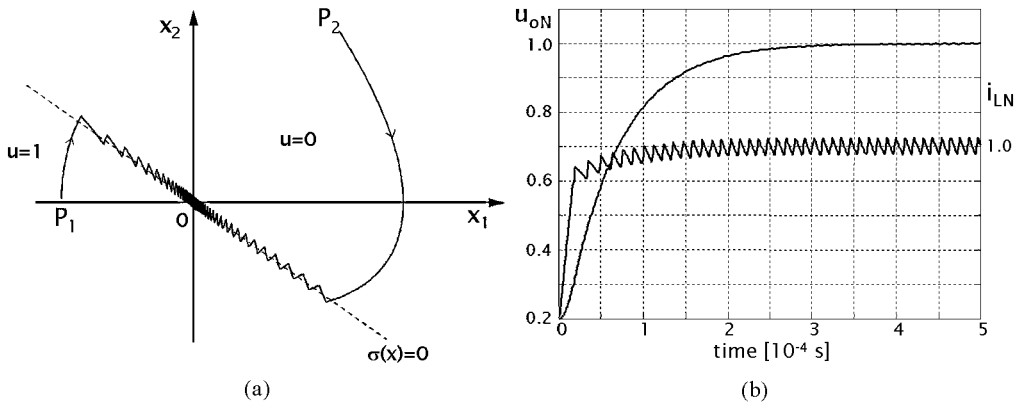

FIGURE 8.6 (a) Phase trajectories for two different initial conditions ($c_1 = 0.8/RC$); (b) Time responses of normalized output voltage u_{oN} and normalized inductor current i_{LN} ($c_1 = 0.8/RC$) (initial conditions in P_1).

Existence Condition

Let us analyze more precisely the existence of the sliding regime for the buck converter. From the sliding-mode theory, the conditions for the sliding regime to exist are (see Eq. 8.9):

$$\dot{\sigma}(\mathbf{x}) = \begin{cases} \mathbf{C}^T\mathbf{A}\mathbf{x} + \mathbf{C}^T\mathbf{B}\mathbf{u}^+ + \mathbf{C}^T\mathbf{D} < 0 & \text{for} \quad 0 < \sigma(\mathbf{x}) < \xi \\ \mathbf{C}^T\mathbf{A}\mathbf{x} + \mathbf{C}^T\mathbf{B}\mathbf{u}^- + \mathbf{C}^T\mathbf{D} > 0 & \text{for} \quad -\xi < \sigma(\mathbf{x}) < 0 \end{cases} \tag{8.27}$$

where ξ is an arbitrary small positive quantity. Using Eqs. (8.22) and (8.24) these inequalities become

$$\begin{cases} \lambda_1(\mathbf{x}) = \left(c_1 - \dfrac{1}{RC}\right)x_2 - \dfrac{1}{LC}x_1 - \dfrac{U_o^*}{LC} < 0 & \text{for} \quad 0 < \sigma(\mathbf{x}) < \xi \\ \lambda_2(\mathbf{x}) = \left(c_1 - \dfrac{1}{RC}\right)x_2 - \dfrac{1}{LC}x_1 + \dfrac{U_g - U_o^*}{LC} > 0 & \text{for} \quad -\xi < \sigma(\mathbf{x}) < 0 \end{cases}$$

Equations $\lambda_1(\mathbf{x}) = 0$ and $\lambda_2(\mathbf{x}) = 0$ define two lines in the phase-plane with the same slope passing through points $(-U_o^*, 0)$ and $(U_g - U_o^*, 0)$, respectively. The regions of existence of the sliding mode are depicted in Fig. 8.7 for two different situations: (1) $c_1 > 1/RC$, and (2) $c_1 < 1/RC$. As we can see, the increase of c_1 value causes a reduction of sliding-mode existence region. Remember that the sliding line coefficient c_1 determines also the system dynamic response in sliding mode, since the system dynamic response results are of first order with a time constant $\tau = 1/c_1$. Thus, high response speeds, i.e., $\tau < RC$, limit the existence region of the sliding mode. This can cause overshoots and ringing during transients.

To better understand this concept, let us take a look to some simulation results. Figure 8.7 shows the phase trajectories of a buck converter with sliding-mode control for two different c_1 values where the initial condition is in $(-U_o^*, 0)$: when the slope of the sliding line becomes too high, as shown in Fig. 8.7a, the system RP hits first the sliding line at a point outside the region of the existence of the sliding mode. As a consequence, the switch remains in a fixed position (open in this case) until the RP hits the sliding line again, now in a region where the existence condition is satisfied.

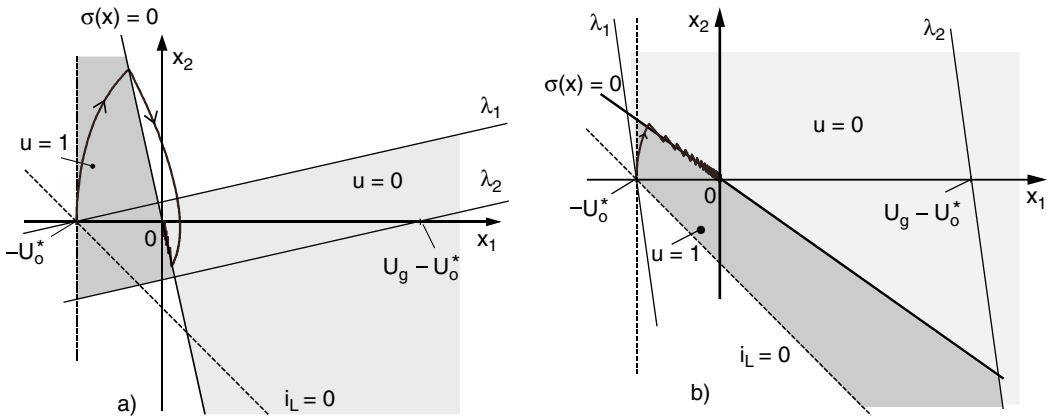

FIGURE 8.7 Regions of existence of the sliding mode in the phase-plane: (a) $c_1 > 1/RC$; (b) $c_1 < 1/RC$.

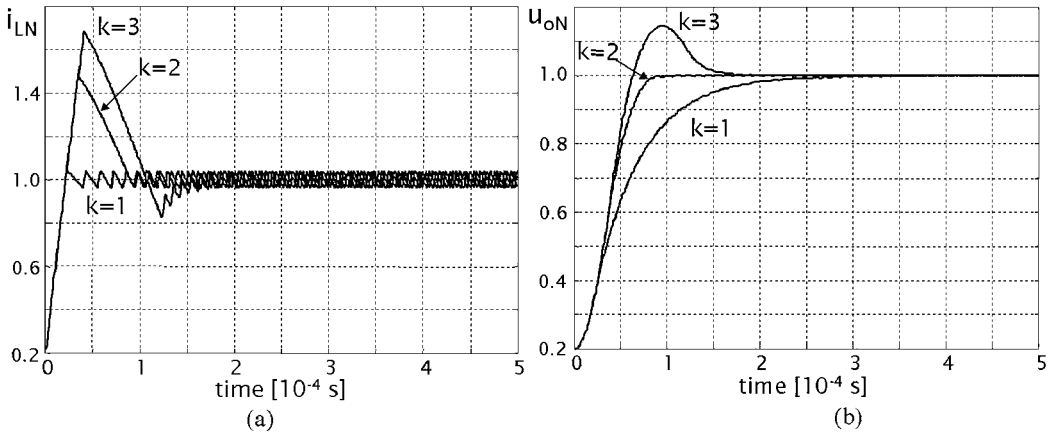

FIGURE 8.8 Time responses of normalized inductor current i_{LN} (a) and normalized output voltage u_{oN} (b) at different c_1 values ($k = c_1$RC).

The time responses of the normalized inductor current i_{LN} and output voltage u_{oN} for different c_1 values are reported in Fig. 8.8a and b respectively ($i_{LN} = i_L/I_o$, $u_{oN} = u_o/U_o$). Note that with $c_1 = 1/\text{RC}$ neither the inductor current nor the output voltage has overshot during start-up.

Current Limitation

As we have seen from Fig. 8.8b, a fast output voltage dynamic calls for overshoots in the inductor current i_L. In fact, the first part of the transient response depends on the system parameters, and only when the system RP hits the sliding line at a point belonging to the existence region is the system dynamic dictated by the sliding equation (for the buck converter it is actually independent of the converter parameters and dependent only on the sliding coefficient c_1). The large inductor current could not be tolerated by the converter devices for two reasons: it can cause the inductor core to saturate with consequent even high-peak current value or can be simply greater than the maximum allowed switch current. Thus, it is convenient to introduce into the controller a protection circuit that prevents the inductor current from reaching dangerous values. This feature can be easily incorporated into the sliding-mode controller by a suitable modification of the sliding line. For example, in the case of buck converters, to keep constant the inductor current we have to force the system RP on the line:

$$x_2 = -\frac{1}{\text{RC}}x_1 + \frac{I_{L\max}}{C} - \frac{U_o^*}{\text{RC}} \tag{8.28}$$

Thus, the global sliding line consists of two pieces:

$$\sigma'(\mathbf{x}) = \begin{cases} \dfrac{x_1}{\text{RC}} + x_2 - \dfrac{1}{C}\left(I_{L\max} - \dfrac{U_o^*}{R}\right) & \text{for} \quad i_L > I_{L\max} \\ c_1 x_1 + x_2 & \text{for} \quad i_L < I_{L\max} \end{cases} \tag{8.29}$$

The phase plane trajectories for a buck converter with inductor current limitation and with $c_1 = 2/\text{RC}$ are shown in Fig. 8.9, and the corresponding normalized inductor current transient behavior is shown in Fig. 8.10. It is interesting to note that Eq. (8.29) gives an explanation of why the fastest response

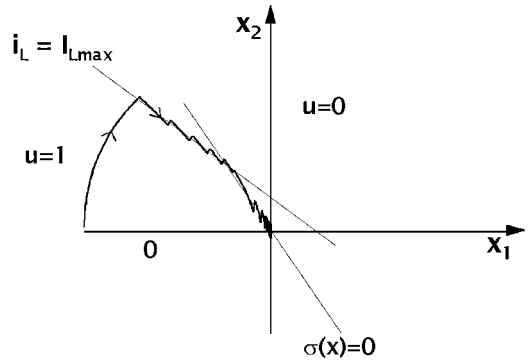

FIGURE 8.9 Phase trajectories for a buck converter with inductor current limitation ($c_1 = 2/RC$).

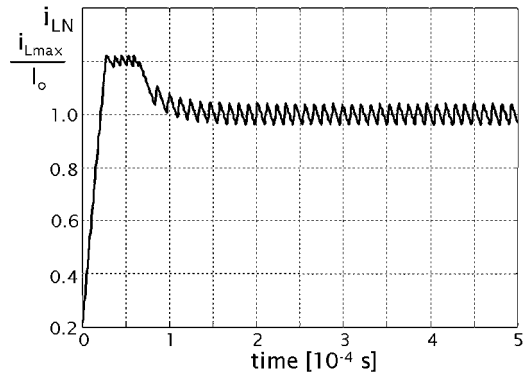

FIGURE 8.10 Time response of normalized inductor current i_{LN} of a buck converter with current limitation ($c_1 = 2/RC$).

without overshoots is obtained for $c_1 = 1/RC$. In fact, if $c_1 = 1/RC$ and $I_{Lmax} = U_o^*/R$ the two pieces of the sliding line σ' become a single line and thus the inductor current reaches its steady-state value U_o^*/R without overshoot.

8.6 Extension to Boost and Buck–Boost DC-DC Converters

For boost as well as buck–boost DC-DC converters, the derivative of the output voltage turns out to be a discontinuous variable, and we cannot express the system in canonical form as was done for the buck converter. Following the general scheme of Fig. 8.3, the inductor current and output voltage errors are chosen as state variables, i.e.,

$$\begin{cases} x_1 = i - I^* \\ x_2 = u_o - U_o^* \end{cases} \tag{8.30}$$

where the current reference I^* depends on the converter operating point (output power and input voltage). Choosing the same control law Eq. (8.26) of the buck converter, together with the following sliding line:

$$\sigma(\mathbf{x}) = x_1 + g x_2 = \mathbf{C}^{\mathrm{T}}\mathbf{x} = 0 \tag{8.31}$$

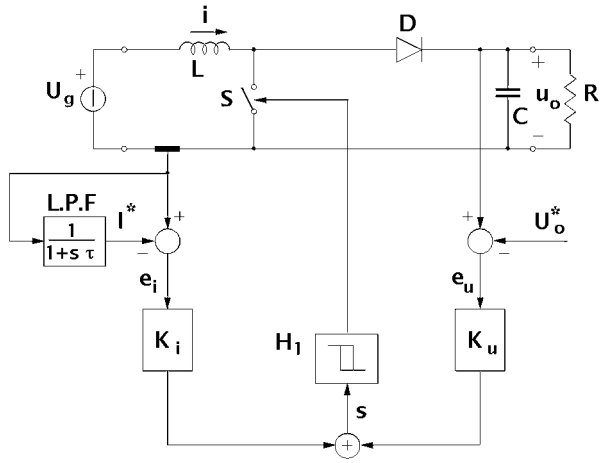

FIGURE 8.11 Boost converter with sliding-mode control.

it can be easily seen [13] that both existence and reaching conditions are satisfied (the former at least in a small region enclosing the origin) as long as

$$g < \frac{\mathrm{RC}}{L}\frac{U_g}{U_o^*} \tag{8.32}$$

for both converters. However, current reference signal I^* is not usually available in practice, and some alternative techniques for its estimation are needed. One possible solution is to derive this reference signal directly from the inductor current by using a low-pass filter, as shown in Fig. 8.11. This estimation clearly affects the dynamic behavior of the sliding-mode control. To understand the closed-loop dynamics of this approach, we need to include the additional state variable introduced by the low-pass filter, i.e.,

$$\frac{di^*}{dt} = -\frac{1}{\tau}i^* + \frac{1}{\tau}i \tag{8.33}$$

Taking into account the boost converter, we can represent the overall system, choosing as state variables:

$$\begin{cases} x_1 = i \\ x_2 = u_o - U_o^* \\ x_3 = i^* \end{cases} \tag{8.34}$$

$$\dot{\mathbf{x}} = \mathbf{A}\mathbf{x} + \mathbf{B}\bar{u} + \mathbf{D} \tag{8.35}$$

$$\mathbf{A} = \begin{bmatrix} 0 & 0 & 0 \\ 0 & -\dfrac{1}{\mathrm{RC}} & 0 \\ \dfrac{1}{\tau} & 0 & -\dfrac{1}{\tau} \end{bmatrix}, \qquad \mathbf{B} = \begin{bmatrix} -\dfrac{u_o}{L} \\ \dfrac{i}{C} \\ 0 \end{bmatrix}, \qquad \mathbf{D} = \begin{bmatrix} \dfrac{U_g}{L} \\ -\dfrac{U_o^*}{\mathrm{RC}} \\ 0 \end{bmatrix}$$

The sliding line becomes a sliding surface in the phase space:

$$\sigma(\mathbf{x}) = x_1 + gx_2 - x_3 = \mathbf{C}^{\mathrm{T}}\mathbf{x} = 0 \tag{8.36}$$

where $\mathbf{C}^{\mathrm{T}} = [1, g, -1]$ is the vector of the sliding surface coefficients and $x_1 - x_3$ represents now the inductor current error. Fortunately, the existence conditions analysis for the system Eq. (8.35) leads to the same constraint (8.32), which can be derived without accounting for the low-pass filter dynamic [13]. However, unlike the buck converter, Eq. (8.32) does not directly give information on the system stability and on the possible values of filter time constant τ.

Stability Analysis

In the following, a procedure similar to the equivalent control method is used to derive a suitable small signal model for the system Eq. (8.35) in sliding mode. The starting point is the *small-signal state space averaged model* of the boost converter [3]:

$$\dot{\hat{\mathbf{x}}} = \mathbf{A}\hat{\mathbf{x}} + \mathbf{B}\hat{u}_g + \mathbf{C}\hat{d} \tag{8.37}$$

$$\mathbf{A} = \begin{bmatrix} 0 & -\dfrac{D'}{L} & 0 \\ \dfrac{D'}{C} & -\dfrac{1}{\mathrm{RC}} & 0 \\ \dfrac{1}{\tau} & 0 & -\dfrac{1}{\tau} \end{bmatrix}, \qquad \mathbf{B} = \begin{bmatrix} \dfrac{1}{L} \\ 0 \\ 0 \end{bmatrix}, \qquad \mathbf{D} = \frac{U_g}{D'} \begin{bmatrix} \dfrac{1}{L} \\ -\dfrac{1}{D'\mathrm{RC}} \\ 0 \end{bmatrix}$$

where $\hat{\mathbf{x}} = [\hat{x}_1, \hat{x}_2, \hat{x}_3]^T = [\hat{i}, \hat{u}_o, \hat{i}^*]^T$ and $D' = 1 - D$. In Eq. (8.37), the dynamic equation of the low-pass filter Eq. (8.33) was added to the original boost equations. From the sliding surface definition we can write:

$$\sigma(\mathbf{x}) = (i - i^*) + g(u_o - U_o^*) = \hat{i} - \hat{i}^* + g\hat{u}_o = \mathbf{C}^{\mathrm{T}}\hat{\mathbf{x}} \tag{8.38}$$

where $\mathbf{C}^{\mathrm{T}} = [1, g, -1]$ and the steady-state values $\mathbf{X}$ of the state variables coincide with the corresponding reference values $\mathbf{X}^*$. Now, if the system is in sliding regime, we can write

$$\sigma(\mathbf{x}) = 0 \Rightarrow \dot{\sigma}(\mathbf{x}) = \mathbf{C}^{\mathrm{T}}\dot{\hat{\mathbf{x}}} = 0 \tag{8.39}$$

From Eqs. (8.37) and (8.39) we can derive an expression for the duty-cycle perturbation as a function of the state variables and the input, which, substituted into Eq. (8.37), yields:

$$\dot{\hat{\mathbf{x}}} = \mathbf{A}'\hat{\mathbf{x}} + \mathbf{B}'\hat{u}_g \tag{8.40}$$

In Eq. (8.40), which represents a third-order system, one equation (for example, the last one corresponding to the variable x_3) is redundant and can be eliminated by using the equation $\sigma = 0$. The result is the

following second-order system:

$$\dot{\hat{\mathbf{x}}} = \mathbf{A_T}\hat{\mathbf{x}} + \mathbf{B_T}\hat{u}_g, \qquad \hat{\mathbf{x}} = [\hat{x}_1, \hat{x}_2]^T \tag{8.41}$$

$$\mathbf{A_T} = \frac{1}{k}\begin{bmatrix} -\dfrac{gD'}{C} & g\left(\dfrac{2}{\mathrm{RC}} - \dfrac{1}{\tau}\right) \\ \dfrac{D'}{C} & \dfrac{1}{\mathrm{RC}}\left(\dfrac{gL}{D'\tau} - 2\right) \end{bmatrix}, \qquad \mathbf{B_T} = \frac{1}{kD'\mathrm{RC}}\begin{pmatrix} -g \\ 1 \end{pmatrix} \quad \text{where} \quad k = 1 - \frac{gL}{D'\mathrm{RC}}$$

Equation (8.41) completely describe the system behavior under sliding mode control. Moreover, they can be used to derive closed-loop transfer functions like output impedance and audiosusceptibility, which allows meaningful comparison with other control techniques. As far as system stability is concerned, by imposing positive values for the coefficients of the characteristic polynomial we obtain

$$0 < g < g_{\mathrm{crit}} = \frac{\mathrm{RC}D'}{L} \tag{8.42}$$

and

$$\tau > \tau_{\mathrm{crit}} = \frac{L}{D'^2 R} \cdot \frac{1}{1 + \dfrac{2}{\mathrm{RD}'g}} \tag{8.43}$$

It is interesting to note that constraint (8.42) coincides with the existence condition given by (8.32).

As an example of application of the discussed analysis, Fig. 8.12 reports the converter audiosusceptibility and output impedance predicted by the model and experimentally measured in a boost converter propotype [13] with the following parameters: $U_g = 24$ V, $U_o = 48$ V, $P_o = 50$ W, $f_s = 50$ kHz, $L = 570$ μH, $C = 22$ μF, $\tau = 0.4$ ms, $g = 0.35$. With this value of sliding coefficient g, the stability analysis shows that the filter time constant τ must be greater than 38 μs for stable operation. Moreover, the chosen value of 400 μs guarantees no output voltage overshoots during transient conditions, as depicted in Fig. 8.13, which reports simulated waveforms of the startup of the boost converter where the output voltage was precharged at the input voltage value.

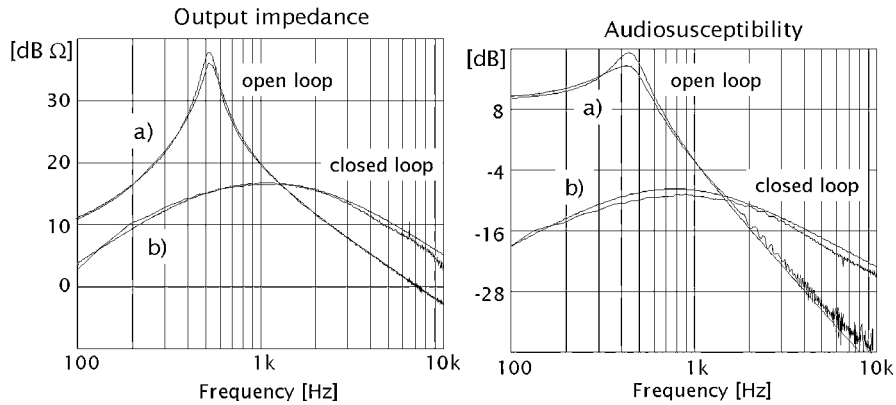

FIGURE 8.12 Comparison between model forecast and experimental results: (a) open loop; (b) closed loop.

TABLE 8.1 Values of τ_{crit} and g_{crit} for Boost and Buck–Boost Topologies

	Boost	Buck–Boost
g_{crit}	$\frac{RCD'}{L}$	$\frac{RC}{L}\frac{D'}{D}$
τ_{crit}	$\frac{L}{D'^2R}\cdot\frac{1}{1+\frac{2}{RD'g}}$	$\frac{L}{\frac{D'^2}{D}R+(2-D')\frac{L}{RC}}$

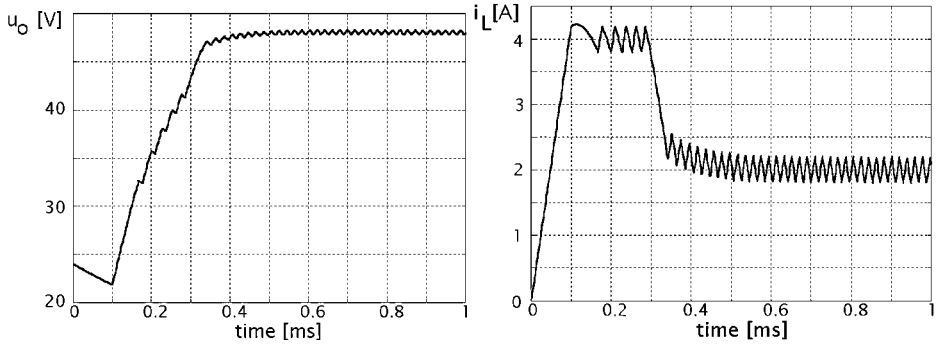

FIGURE 8.13 Output voltage and inductor current at startup of a boost converter (output capacitor precharged at input voltage).

The same stability analysis can be applied also to buck–boost converters. As a result, the critical value for the low-pass filter time constant τ_{crit} and g_{crit} are given in Table 8.1.

8.7 Extension to Cúk and SEPIC DC-DC Converters

As a general approach to high-order converters like Cúk and SEPIC, a sliding function can be built as a linear combination of all state variable errors x_i, i.e., $\sigma(\mathbf{x}) = \Sigma_{i=1}^{N} c_i x_i$, as depicted in Fig. 8.3. This general approach, although interesting in theory, is not practical. In fact, it requires sensing of too many state variables with an unacceptable increase of complexity as compared with such standard control techniques as current-mode control. However, for Cúk and SEPIC converters a reduced-order sliding-mode control can be used with satisfactory performances with respect to standard control techniques [9–11]. In this case, some sliding coefficients are set to zero. In particular, for Cúk and SEPIC converters, the sensing of only output voltage and input inductor current was proposed and the current reference signal was obtained, as for the boost and buck–boost converter, by using a low-pass filter. Taking the SEPIC converter as an example, the resulting scheme with reduced-order implementation is reported in Fig. 8.14. Of course, the same scheme can be applied to Cúk converters as well.

To give design criteria for selection of sliding-mode controller parameters, the system must be represented in a suitable mathematical form. To this purpose, the converter equations related to the two subtopologies corresponding to the switch status are written as

$$\dot{\mathbf{v}} = \mathbf{A}_{on}\mathbf{v} + \mathbf{F}_{on} \qquad \text{switch on,} \tag{8.44}$$

$$\dot{\mathbf{v}} = \mathbf{A}_{off}\mathbf{v} + \mathbf{F}_{off} \qquad \text{switch off,} \tag{8.45}$$

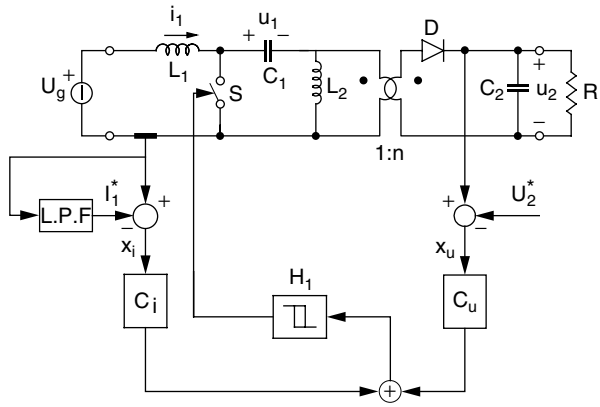

FIGURE 8.14 SEPIC converter with sliding-mode control.

where $\mathbf{v} = [i_1, i_2, u_1, u_2]^T$ is the state variable vector. These equations are combined in the following form (VSS)

$$\dot{\mathbf{v}} = \mathbf{A}\mathbf{v} + \mathbf{B}u + \mathbf{F}, \tag{8.46}$$

where u is the discontinuous variable corresponding to the switch status and matrices $\mathbf{A}, \mathbf{B}, \mathbf{F}$ are given by

$$\mathbf{A} = \mathbf{A}_{\text{off}}, \quad \mathbf{F} = \mathbf{F}_{\text{off}}, \tag{8.47}$$

$$\mathbf{B} = (\mathbf{A}_{\text{on}} - \mathbf{A}_{\text{off}})\mathbf{v} + (\mathbf{F}_{\text{on}} - \mathbf{F}_{\text{off}}) \tag{8.48}$$

It is convenient to write the system Eq. (8.47) in terms of state variables error x_i, where $\mathbf{x} = \mathbf{v} - \mathbf{V}^*$, being $\mathbf{V}^* = [I_1^*, I_2^*, U_1^*, U_2^*]^T$ the vector of state variable references. Accordingly, system equations become

$$\dot{x} = Ax + Bu + G, \tag{8.49}$$

where $G = AV^* + F$.

Existence Condition

Assuming that the switch is kept on when σ is negative and off when σ is positive, we may express the existence condition in the form (see Eq. 8.9):

$$\begin{aligned} \frac{\partial \sigma}{\partial t} &= C^T Ax + C^T G < 0 \qquad 0 < \sigma < \xi \\ \frac{\partial \sigma}{\partial t} &= C^T Ax + C^T B + C^T G > 0 \qquad -\xi < \sigma < 0, \end{aligned} \tag{8.50}$$

where ξ is an arbitrary small positive quantity. Inequalities (8.50) are useful only if state variable errors x_i are bounded; otherwise, (8.50) must be analyzed under small-signal assumption. In this latter case, satisfying (8.50) means enforcing the existence condition in a small volume around the operating point, and this is equivalent to ensuring the stability condition as demonstrated in Ref. 13.

Hitting Condition

If sliding mode exists, a sufficient hitting condition is

$$C^T A_4 \leq 0 \tag{8.51}$$

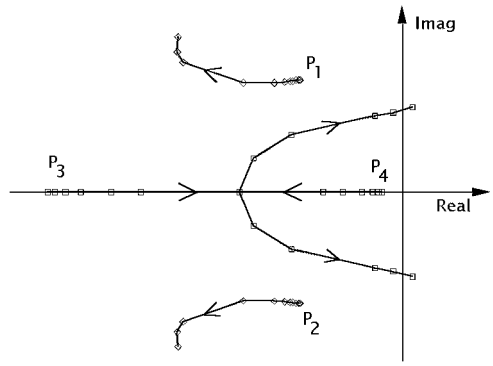

FIGURE 8.15 Root locus of closed-loop system for variation of low-pass filter time constant of the SEPIC converter [13].

where A_4 is the fourth column of matrix **A** [1, 2]. This yields the following constraint

$$-\frac{c_i}{nL_1} - \frac{c_u}{R_L C_2} \leq 0 \tag{8.52}$$

where c_i and c_u are the sliding line coefficients for the input current and output voltage errors, respectively, and n is the ratio between the second and the primary transformer windings.

Stability Condition

This issue must be addressed taking into account the effect of the time constant τ of the low-pass filter needed to extract the inductor current reference signal. To this purpose the small-signal analysis carried out for the sliding-mode control of boost converters can be generalized [13]. This can be used to derive useful design hints for the selection of sliding surface coefficients and filter time constants. As an example, from the small signal model in sliding mode, similar to (8.41), the root locus of closed-loop system eigenvalues can be plotted as a function of the low-pass filter time constant as shown in Fig. 8.15 in the case of a SEPIC converter [11]. Note that the system become unstable for low value of time constant τ. A similar analysis can be applied to Cúk converters as well.

8.8 General-Purpose Sliding-Mode Control Implementation

Compared to the current control, the sliding-mode approach has some aspects that still must be improved. The first problem arises from the fact that the switching frequency depends on the rate of change of function σ and on the amplitude of the hysteresis band. Since σ is a linear combination of state-variable errors, it depends on actual converter currents and voltages, and its behavior may be difficult to predict. This can be unacceptable if the range of variation becomes too high. One possible solution of the problem related to the switching frequency variations is the implementation of a variable hysteresis band, for example, using a PLL (phase locked loop). Another simple approach is to inject a suitable constant-frequency signal w into the sliding function as shown in Fig. 8.16 [10]. If, in the steady state, the amplitude of w is predominant in σ_f, then a commutation occurs at any cycle of w. This also allows converter synchronization to an external trigger. Instead, under dynamic conditions, error terms x_i and x_u increase, w is overridden, and the system retains the excellent dynamic response of the sliding mode. Simulated waveforms of ramp w, and σ_{PI}, σ_f signals are reported in Fig. 8.17.

The selection of the ramp signal w amplitude is worthy of further discussion. In fact, it should be selected by taking into account the slope of function σ_{PI} and the hysteresis band amplitude, so that function σ_f hits the lower part of the hysteresis band at the end of the ramp, causing the commutation. From the analysis of the waveform shown in Fig. 8.17, we can find that the slope S_e of the external ramp

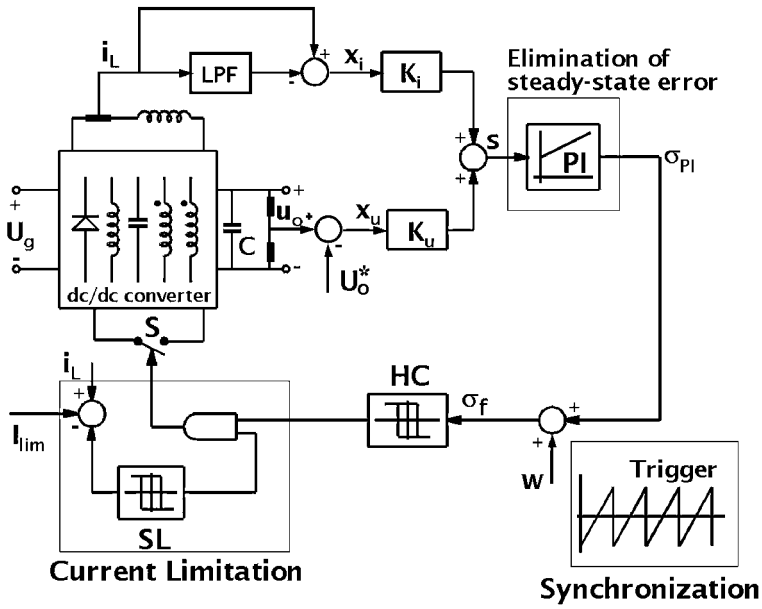

FIGURE 8.16 Reduced-order sliding-mode controller with inductor current limitation, constant switching frequency, and no output voltage steady-state error.

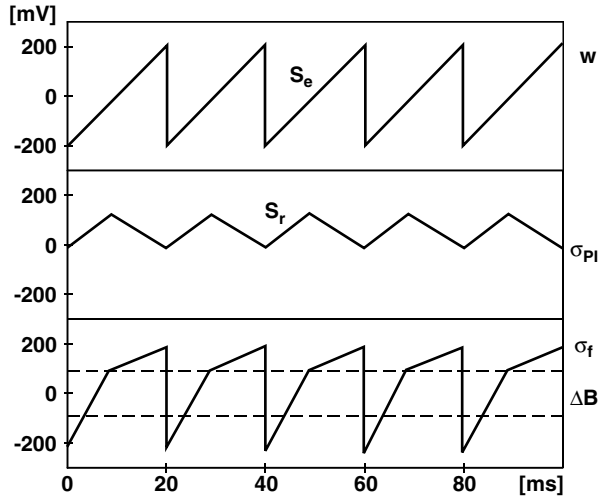

FIGURE 8.17 Simulated waveforms of ramp w, and σ_{PI}, σ_f signals.

must satisfy the following inequality

$$S_e > \frac{\Delta B}{\delta T_s} - S_r \tag{8.53}$$

where ΔB represents the hysteresis band amplitude and S_r is the slope of function σ_{PI} during the switch on-time. Note that, in the presence of an external ramp, signal σ_{PI} must have a nonzero average value to accommodate the desired converter duty cycle (see Fig. 8.17). Of course, a triangular disturbing signal w is not the only waveform that can used. A pulse signal has been used alternatively as reported in Ref. 12.

The second problem derives from a possible steady state error on the output voltage. In fact, when the inductor current reference is evaluated using a low-pass filter, then the current error leads naturally to zero average value in steady state. Thus, if the sliding function, due to the hysteretic control or due to the added ramp signal w, has nonzero average value, a steady-state output voltage error necessarily appears. This problem can be solved by introducing a PI action on sliding function to eliminate its DC value (see Fig. 8.16). In practice, the integral action of this regulator is enabled only when the system is on the sliding surface; in this way, the system behavior during large transients, when σ can have values far from zero, is not affected, thus maintaining the large-signal dynamic characteristics of sliding-mode control. A general-purpose sliding-mode controller scheme that includes the aforementioned improvements, together with reduced-order implementation in the case of Cúk and SEPIC converters and a possible implementation of current limitation by means of another hysteretic comparator and an AND port, is reported in Fig. 8.16. Experimental results of this scheme are reported in Refs. 10 and 11.

8.9 Conclusions

Control techniques of VSS find a natural application to SMPS, since they inherently show variable structure properties as a result of the conversion process and switch modulation. Thus, the sliding-mode control represents a powerful tool to enhance performance of power converters. Sliding-mode control is able to ensure system stability even for large supply and load variations, good dynamic response, and simple implementation, even for high-order converters. These features make this control technique a valid alternative to standard control approaches.

The application of the sliding-mode control technique to DC-DC converters is the focus of this chapter. The application to buck converters is discussed in detail, whereas for the extension of this control technique to boost, buck–boost, Cúk, and SEPIC converters only some design guidelines are given. Finally, such improvements as current limitation, constant switching frequency, and output voltage steady-state error cancellation are outlined. This control approach can also be effectively used in other applications, not discussed here, such as inverters [14, 18], power factor controllers [16], and AC power supplies [17].

References

1. V. I. Utkin, *Sliding Modes and Their Application in Variable Structure Systems,* MIR Publishers, Moscow, 1978.
2. U. Itkis, *Control Systems of Variable Structure,* John Wiley & Sons, New York, 1976.
3. R. D. Middlebrook and S. Cuk, *Advances in Switched-Mode Power Conversion,* Vol. I and II, TESLAco, Pasadena, CA, 1983, 73–89.
4. R. Redl and N. Sokal, Current-mode control, five different types, used with the three basic classes of power converters: small-signal AC and large-signal DC characterization, stability requirements, and implementation of practical circuits, in *IEEE-PESC,* 1985, 771–785.
5. J. G. Kassakian, M. F. Schlecht, and G. C. Verghese, *Principles of Power Electronics,* Addison-Wesley, Reading, MA, 1991.
6. R. Venkataramanan, A. Sabanovic, and S. Cúk, Sliding-mode control of DC-to-DC converters, in *IECON Conf. Proc.,* 1985, 251–258.
7. B. Nicolas, M. Fadel, and Y. Chéron, Robust control of switched power converters via sliding mode, *ETEP,* 6(6), 413–418, 1996.
8. B. Nicolas, M. Fadel, and Y. Chéron, Sliding mode control of DC-to-DC converters with input filter based on Lyapunov-function approach, in *EPE Conf. Proc.,* 1995, 1.338–1.343.
9. L. Malesani, L. Rossetto, G. Spiazzi, and P. Tenti, Performance optimization of Cúk converters by sliding-mode control, *IEEE Trans. Power Electron.*, 10(3), 302–309, 1995.
10. P. Mattavelli, L. Rossetto, G. Spiazzi, and P. Tenti, General-purpose sliding-mode controller for DC/DC converter applications, in *Proc. of IEEE Power Electronics Specialists Conf. (PESC)*, Seattle, June 1993, 609–615.

11. P. Mattavelli, L. Rossetto, G. Spiazzi, and P. Tenti, Sliding mode control of SEPIC converters, in *Proc. of European Space Power Conf. (ESPC),* Graz, August 1993, 173–178.
12. J. Fernando Silva and Sonia S. Paulo, Fixed frequency sliding mode modulator for current mode PWM inverters, in *Power Electronics Specialists Conf. Proc. (PESC),* 1993, 623–629.
13. P. Mattavelli, L. Rossetto, and G. Spiazzi, Small-signal analysis of DC-DC converters with sliding mode control, *IEEE Trans. Power Electron.,* 12(1), 79–86, 1997.
14. N. Sabanovic, A. Sabanovic, and K. Ohnishi, Sliding mode control of three-phase switching converters, in *Proc. of Int. Conf. on Industrial Electronics, Control and Instrumentation (IECON),* San Diego, 1992, 319–325.
15. N. Sabanovic-Behlilovic, A. Sabanovic, and T. Ninomiya, PWM in three-phase switching converters-sliding mode solution, in *Power Electronics Specialists Conference, PESC '94 Record, 25th Annual IEEE,* Vol. 1, 1994, 560–565.
16. L. Rossetto, G. Spiazzi, B. Fabiano, and C. Licitra, Fast-response high-quality rectifier with sliding mode control, *IEEE Trans. Power Electron.,* 9(2), 146–152, 1994.
17. L. Malesani, L. Rossetto, G. Spiazzi, and A. Zuccato, An AC power supply with sliding-mode control, *IEEE Ind. Appl. Mag.,* 2(5), 32–38, 1996.
18. H. Pinheiro, A. S. Martins, and J. R. Pinheiro, A sliding mode controller in single phase voltage source inverters, in *IEEE IECON '94,* 1994, 394–398.
19. H. Sira-Ramirez and M. Rios-Bolivar, Sliding mode control of DC-to-DC power converters via extended linearization circuits and systems I: fundamental theory and applications, *IEEE Transactions on Circuits and Systems* 41(10), 652–661, 1994.